sciendo

Polish Journal of Chemical Technology, 25, 1, 12—19, 10.2478/pjct-2023-0003

Synthesis of nanoscale zero-valent iron doped carbonized zeolitic imidazolate framework-8 for methylene blue removal in water

Shuai Chen[1, 2], Lemeng Qiao[1], Xuejiao Feng[1], Yufu Huang[3], Guilan Gao[1], Jie Guan[1], Donghai Lin[3, *]

[1]*School of Resources and Environmental Engineering, Shanghai Polytechnic University, Shanghai 201209, China*
[2]*Anhui International Joint Research Center for Nano Carbon-based Materials and Environmental Health, Huainan, 232001, China*
[3]*School of Energy and Materials, Shanghai Polytechnic University, Shanghai Engineering Research Center of Advanced Thermal Functional Materials, Shanghai Key Laboratory of Engineering Materials Application and Evaluation, Shanghai 201209, China*
[*]*Corresponding author: e-mail: dhlin@sspu.edu.cn*

Nanoscale zero-valent iron-doped carbonized zeolitic imidazolate framework-8 (nZVI/CZIF-8) was prepared by carbonation of ferric nitrate and ZIF-8 at 800 °C and used as an adsorbent to remove methylene blue (MB) from water. The synthesized nZVI/CZIF-8 has a specific surface area of 806.9 m^2/g, a pore volume of 0.86 cm^3/g and an nZVI content of 1.35%, respectively. Both the nZVI/CZIF-8 and CZIF-8 have identical functional groups of O-H, C-H and C=C. With the increase of CZIF-8 size, MB removal rate increased. The doping of nZVI increased the MB removal percentage from 74.5% for ZIF-8 to 96.2% within 80 min for nZVI/CZIF-8. The MB removal percentage increased with the dosage of nZVI/CZIF-8. The MB adsorption with the adsorbents conforms to the Freundlich adsorption isothermal model and the removal rate fitted well to a pseudo-first-order model. The results demonstrate the feasibility of synthesizing high active and stable nZVI/CZIF-8 particles.

Keywords: Nanoscale zero-valent iron; Carbonized zeolitic imidazolate framework-8; Mesoporous carbon; Methylene blue.

INTRODUCTION

Dyes are commonly used in industries including textile, paper, leather, plastics, etc., while 95% of them are discharged and will cause serious harm to the environment and ecosystem[1–6]. Among these, methylene blue (MB), the most commonly used dye for coloring wood, cotton, and silk, can lead to adverse reactions such as permanent injury to the eyes and respiratory system[7, 8]. Among the methods to remove MB from wastewater, adsorption is the most promising one because of its efficiency[9–11]. Adsorbents, including biochar, activated carbon, graphene, clay, lignin, pine, $Na_2Ti_3O_7$, etc., have been applied to remove MB from water[9, 12–17]. Recently, mesoporous carbon materials have attracted interest in adsorption processes[18, 19]. For example, Wang et al.[20] synthesized magnetic mesoporous carbon nanospheres by pyrolyzing iron-phenolic coordination polymer with tannic acid and used them as adsorbents for Cr(VI) removal. Krebsz et al.[21] prepared bio-graphene foam to remove chromate ion removal and oil-water separation. Pasinszki et al.[22] synthesized nanofurry magnetic carbon microspheres for separation and catalysis processes.

Nanoscale zero-valent iron (nZVI) is a robust reagent that could remove pollutants via reduction, oxidation, specific retention and (co)precipitation mechanisms[23]. Previous studies have used nZVI to remove MB from water[24–26]. The intrinsic disadvantages of nZVI are surface passivation and aggregation between particles, which often reduce its efficiency[23]. An effective strategy is to disperse nZVI particles on carbonaceous materials[27]. The existence of carbon materials could decrease the oxidation rate of nZVI through non-targeted oxidation processes and improve electron transfer[28, 29]. Shi et al.[30] obtained nZVI-doped mesoporous carbon by reducing $Fe(NO_3)_3{\cdot}9H_2O$ by H_2 during pyrolysis of carbon precursor. The resultant material reveals enhanced stability and mobility in aqueous solution and porous media, as well as effective nickel diffusion and reactions. Baikousi et al.[31] synthesized nZVI supported on commercial mesoporous carbon by reducing Fe^{3+} ions in water with sodium borohydride. Carbon microspheres containing nZVI on their surface were synthesized by carbonizing polystyrene–divinylbenzene-based, iron nitrate-loaded ion exchange resins[22]. However, nZVI on carbon support materials is not tight, leading to the weak stability of these materials in aqueous phase.

Zeolitic imidazolate framework-8 (ZIF-8), as a typical metal-organic framework (MOF), can be easily and effectively prepared[32, 33]. It has been reported that ZIF-8 has a sodalite-type structure, micropores, high thermal stability (up to 400 °C), and a symmetrical relationship with hydrophobicity[34]. This MOF has been extensively studied for gas separation, H_2 storage, encapsulation and catalysis[35]. As a MOF, ZIF-8 can be directly carbonized without adding carbon source. In this study, $Fe(NO_3)_3{\cdot}9H_2O$ was used as the source of nZVI to prepare nZVI-doped carbonized ZIF-8 (nZVI/CZIF-8) by carbothermal reduction during ZIF-8 pyrolysis. This process makes the nZVI particles stay tight in carbon material and could obtain stable supported nZVI material, which is benefit to its application in soil and water remediation. Herein, nanoscale zero-valent iron-doped carbonized zeolitic imidazolate framework-8 (nZVI/CZIF-8) was prepared by carbonation of ferric nitrate and ZIF-8 at 800 °C and used as an adsorbent to remove methylene blue (MB) from water. The structural and textural properties were analyzed by X-ray diffraction (XRD), scanning probe microscope (SPM), energy dispersive spectroscopy (EDS), Fourier transform infrared spectroscope (FTIR), Raman spectroscope and N_2 adsorption-desorption. MB was used as a model pollutant

to test the pollutant removal activities and kinetics of CZIF-8 and nZVI/CZIF-8 in water (Scheme 1). To the best of our knowledge, it is the first time to synthesize nZVI/CZIF-8 with Fe(III) doped ZIF-8 for MB removal in water.

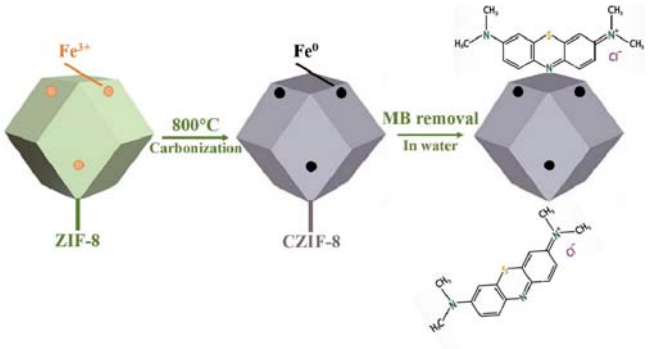

Scheme 1. The preparation of nZVI/CZIF-8

MATERIALS AND METHODS

Chemicals

$Fe(NO_3)_3{\cdot}9H_2O$ (>98.5%), $Zn(NO_3)_2{\cdot}6H_2O$ (>99%), 2-methylimidazole (>98%), methanol (>99.5%), absolute ethyl alcohol (>99.7%) and methylene blue (>98%) were obtained from Sinopharm Chemical Reagent Co., Ltd. (Shanghai, China).

Synthesis and characterization of CZIF-8 and nZVI/CZIF-8

CZIF-8 was prepared in several steps. Firstly, mixing 3.39 g of $Zn(NO_3)_2{\cdot}6H_2O$ with 300 mL methanol, and 3.94 g of 2-methylimidazole with another 300 mL methanol, respectively, in two beakers, and stirring evenly with glass sticks. Then pouring the above mixture into a 1 L beaker, stirring it well with a glass stick, and heating it in a water bath at 60 °C for 24 h. The above solution was centrifuged (8000 rpm/min) for 3 min and washed with ethanol (9000 rpm/min) for 2 min. After that, the obtained precipitate was put into a vacuum-drying furnace at 60 °C for 24 h. The final precipitate was put into the quartz boat and then heated in the tubular furnace for 1 h (constant temperature time) at the temperatures of 800, 900 and 1000 °C in a nitrogen atmosphere to obtain carbonized ZIF-8 (CZIF-8). CZIF-8 with different sizes can be obtained by adjusting the amount of methanol (100, 300 and 600 mL). To obtain nZVI/CZIF-8, just mix 100 mg $Fe(NO_3)_3{\cdot}9H_2O$ with 3.39 g $Zn(NO_3)_2{\cdot}6H_2O$ in the first step of preparing CZIF-8.

The crystalline structure of CZIF-8 and nZVI/CZIF-8 was characterized by XRD using a BRUKER AXS GMBH D8 diffractometer. The surface morphology of CZIF-8 and nZVI/CZIF-8 was observed by SPM using a Shimadzu SPM-9600 microscope. The elemental compositions were analyzed using an EDAX TEAM Apollo EDS. Textural analyses of materials were performed by the N_2 adsorption-desorption method at –196 °C using a Micromeritics TriStar 123 static volumetric system. The samples were previously outgassed under vacuum at 150 °C for 2 h, and the specific surface area was estimated by the Brunauer–Emmett–Teller (BET) method. The pore size distribution in nZVI/CZIF-8 was obtained by the Barrett–Joyner–Halenda (BJH) method. The functional groups of the nZVI/CZIF-8 were studied by the Thermo Electron Group Nicolet 6700 FTIR spectrometer in a frequency range of 400–4000 cm^{-1} using KBr pellet method. The Raman spectra of nZVI/CZIF-8 were acquired on a BRUKER SENTERRA Raman system with a 633 nm He–Ne laser.

Removal of MB in water with CZIF-8 and nZVI/CZIF-8

MB removal tests were carried out in 150 mL conical flasks at 20 °C containing 100 mL MB solution (20 mg/L) and a certain amount of CZIF-8 or nZVI/CZIF-8 in a table concentrator (150 rpm). At given time intervals, 3.5 mL of the solution was collected and analyzed by Meipuda UV-1800PC UV-vis spectrophotometer (Shanghai, China), with the scanning range between 650–680 nm and the thickness of the colorimetric dish was 1 cm. All the experiments detailed above were performed in triplicate and the average values are reported.

The MB adsorption and removal results with various materials can be fitted with Langmuir (Eq. 1), Freundlich (Eq. 2) and pseudo-first-rate (Eq. 3) models:

$$C_e/Q_e = C_e/Q_m + 1/(Q_m{\cdot}K_L) \quad (1)$$

$$ln(Q_e) = ln(K_F) + 1/(n{\cdot}KF) \quad (2)$$

$$-ln(C_t/C_0) = k_1{\cdot}t \quad (3)$$

where Q_e is the amount of MB absorbed at equilibrium concentration (mg/g), C_e is the equilibrium concentration of MB in solution (mg/L), K_L is the Langmuir constant (L/mg), Q_m is the maximum monolayer sorption capacity (mg/g), K_F and n are Freundlich constants, C_t is the MB concentration in solution at time t, C_0 is the initial MB concentration.

3. RESULTS AND DISCUSSIONS

Size controlling of CZIF-8

The amount of methanol plays an important role in the size of CZIF-8 material. Fig. 1 reveals the SEM images of CZIF-8 with the methanol amount of 100 mL, 300 mL and 600 mL, respectively. The particle size of CZIF-8 using 100 mL methanol is about 1 μm (Fig. 1a). As the methanol amount increases to 300 mL, the particle size decreases to about 200 nm (Fig. 1b). Then, CZIF-8 particles with size of 100 nm can be obtained by adding 600 mL methanol (Fig. 1c).

Characterization of CZIF-8 and nZVI/CZIF-8

The XRD patterns of CZIF-8 materials are shown in Fig. 2a. The diffraction peaks around $2\theta = 24^o$ and $2\theta = 44^o$ correspond to the (002) and (100) planes of graphitic carbon, and the broad peaks indicate that the main structure of the material is amorphous carbon type[36]. Further, some researchers define these two peaks as characteristic peaks of reduced graphene oxide and strutted graphene[21, 37, 38]. The XRD results of CZIF-8 and nZVI/CZIF-8 prepared at various temperatures are shown in Fig. 2b. After heating at a temperature higher than 800 °C, nZVI/CZIF-8 can be successfully synthesized. The XRD results of nZVI/CZIF-8 show a new peak at about $2\theta = 46.7^o$, which maybe corresponds to the formation of Fe^0 through Eqs. 4–6. It is noteworthy that nZVI can be synthesized at 800 °C, which is lower than that reported in our previous study[29]. The existence of Fe_3O_4 peaks in the XRD results of nZVI/CZIF-8

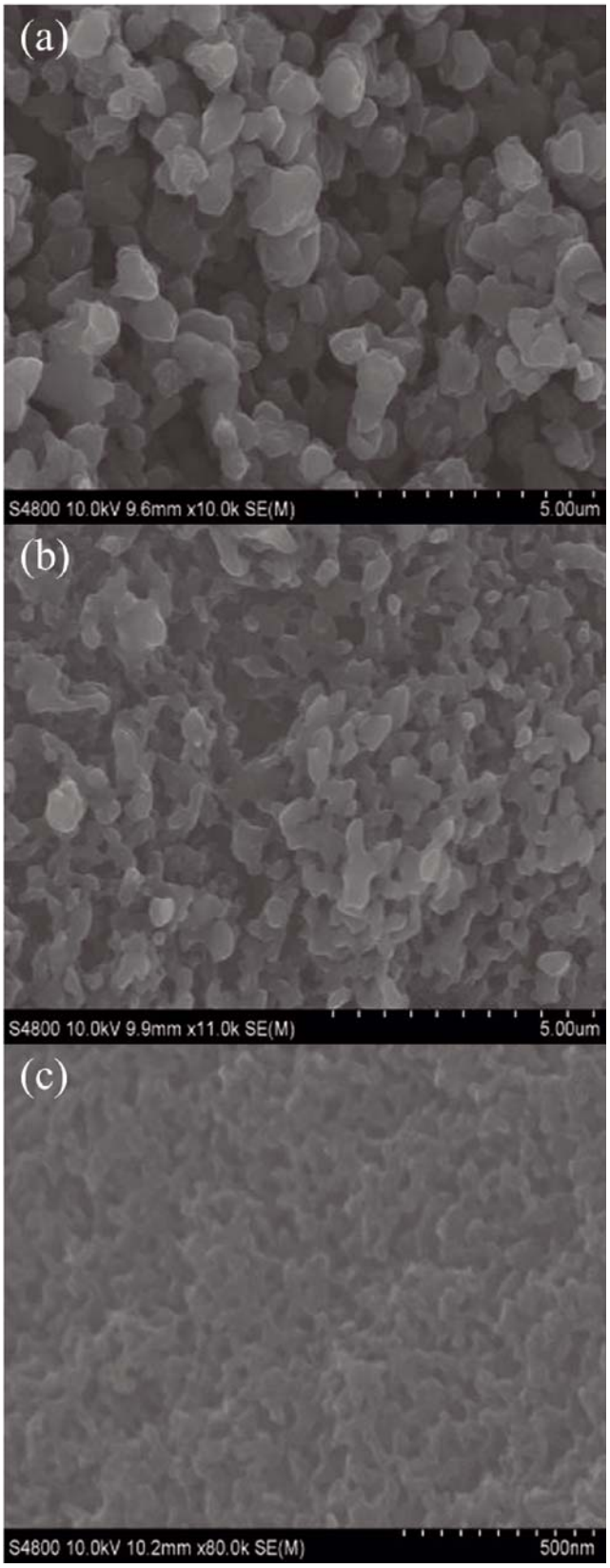

Figure 1. SEM images of CZIF-8 with 100 mL (a), 300 mL (b) and 600 mL (c) methanol

synthesized at higher temperature may be due to the oxidation of nZVI when preparing samples[39].

$$3C + Fe_2O_3 \rightarrow 3CO \uparrow + 2Fe \quad (4)$$

$$3C + 2\ Fe_2O_3 \rightarrow 3CO_2 \uparrow + 2Fe \quad (5)$$

$$3CO + Fe_2O_3 \rightarrow 3CO_2 \uparrow + 2Fe \quad (6)$$

Figure 3a illustrates the FTIR patterns of CZIF-8 and nZVI/CZIF-8 with almost the same typical peaks. The peak near 1560 cm^{-1} is C=C skeleton vibration. The absorption peak at 2330 cm^{-1} is generated by the asymmetric stretching vibration of O=C=O, which may be due to the CO_2 from air adsorbed on the sample. Further, the peak at 3420 cm^{-1} is caused by the stretching vibration of O-H because of the water adsorbed from air when preparing samples[40]. These results show that the organic matrix was destroyed because of the carbonization during the heat treatment. The synthesized nZVI/CZIF-8 still retains the characteristic functional groups of CZIF-8. However, due to the low content of iron, the characteristic peak of the Fe-O was not detected[39]. The Raman pattern of CZIF-8 is shown in Fig. 3b, the peak at 1350 cm^{-1} is D band of carbon materials, while the one at 1600 cm^{-1} is the G band. The D band represents the disorder degree of materials, while G band represents the graphitization degree of materials[41, 42]. The integral strength ratio I_D/I_G = 1.04, indicating that the prepared ZIF-8 has some graphitization structure, but there is larger amount of amorphous carbon structures[43]. Fig. 4 provides the SEM (Fig. 4a) and SEM-EDS (Fig. 4b-d) results of nZVI/CZIF-8. The SEM image of nZVI/CZIF-8 illustrates that the particles have a uniform size of about 100 nm. The SEM-EDS results reveal that the nZVI particles are dispersed with the CZIF-8 particles. These results, combined with the XRD results, demonstrate that the nZVI/CZIF-8 adsorbent was synthesized successfully.

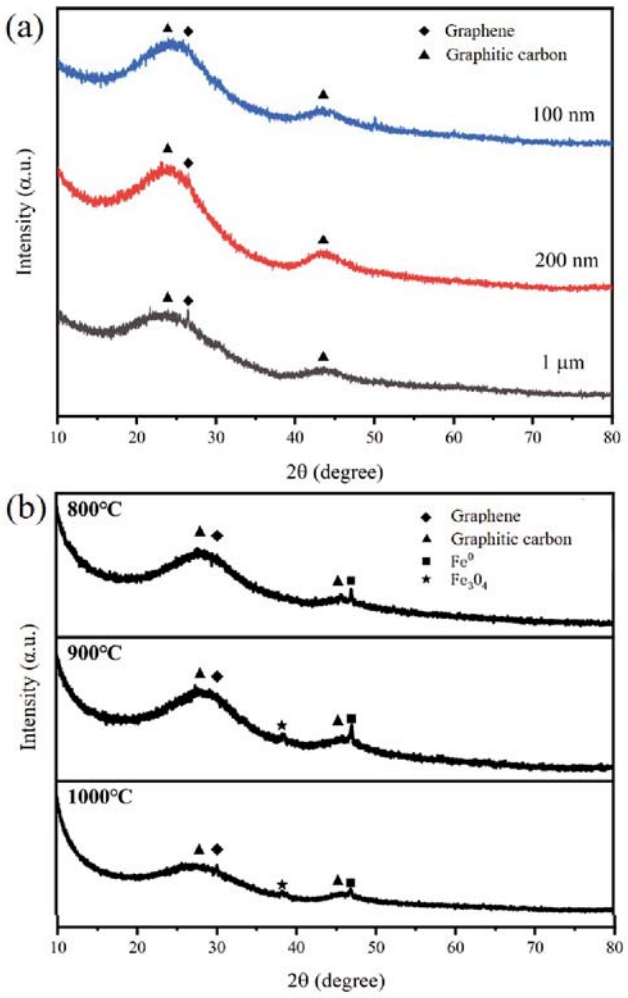

Figure 2. XRD patterns of CZIF-8 and nZVI/CZIF-8

Figure 5a depicts the N_2 adsorption-desorption curves of nZVI/CZIF-8, which is a type IV isotherm with an H4 hysteresis ring, implying the mesoporous nature of nZVI/CZIF-8[39, 44]. The BET specific surface area and

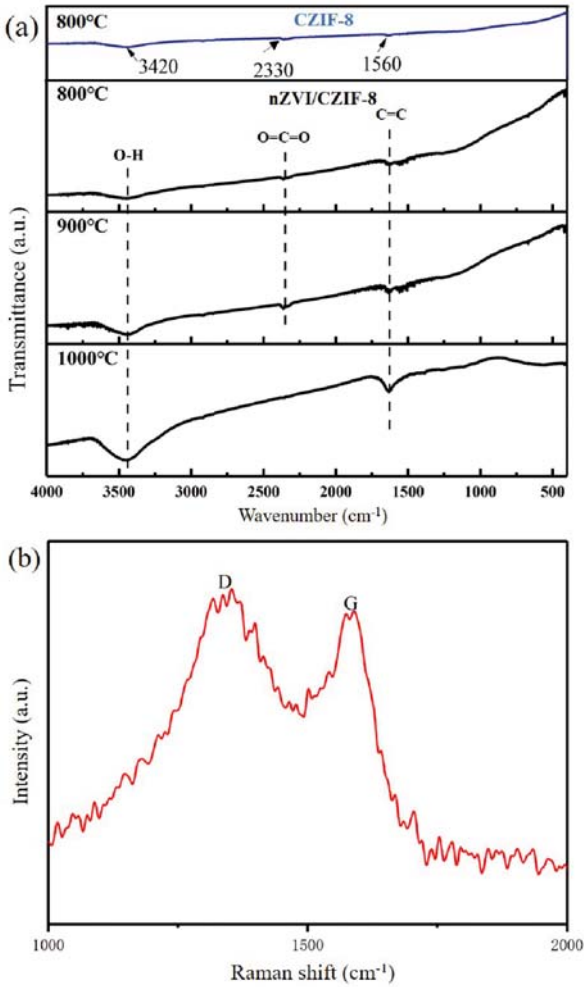

Figure 3. FTIR spectra of CZIF-8 and nZVI/CZIF-8 (a), and Raman spectra of CZIF-8 (b)

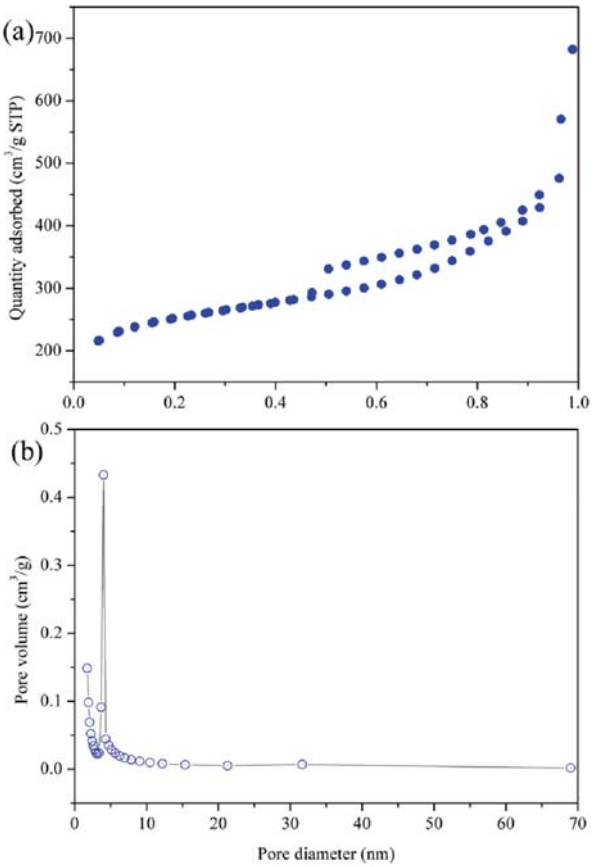

Figure 5. N_2 adsorption-desorption curves (a) and pore volume distribution (b) of nZVI/CZIF-8

Table 1. Textural characteristics of nZVI/CZIF-8

S_{BET} (m^2/g)	$S_{Langmuir}$ (m^2/g)	S_{BJH} (m^2/g)	Pore volume (cm^3/g)	Pore size (nm)
806.9	1213.4	807.6	0.86	5.2

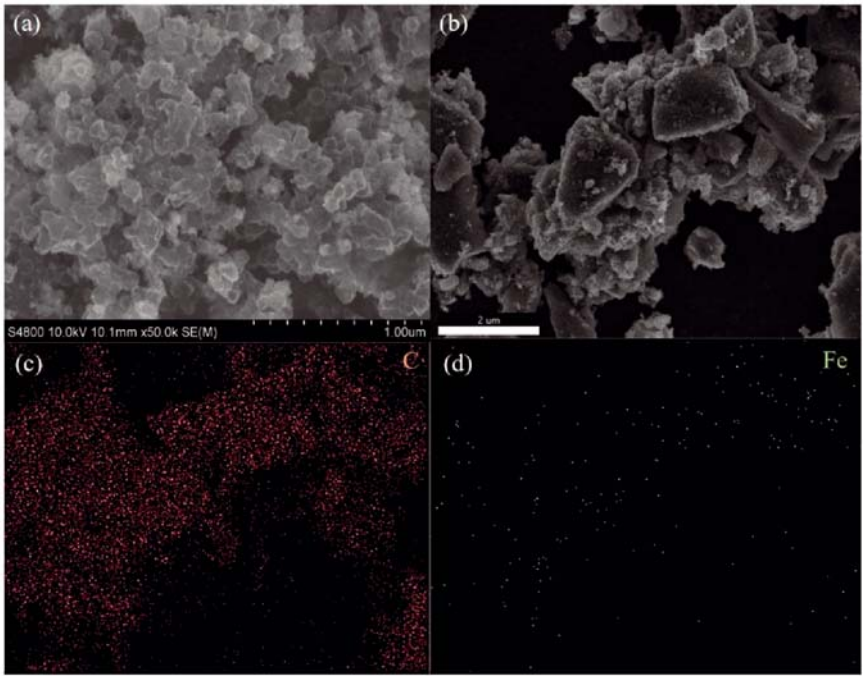

Figure 4. SEM (a) and SEM-EDS (b-d) results of nZVI/CZIF-8

pore volume of nZVI/CZIF-8 are 806.9 m^2/g and 0.86 cm^3/g, respectively, which reveals the high specific surface area and pore volume as the synthesized ZIF-8 materials reported in previous studies[45, 46]. Fig. 5b indicates the pore distribution of nZVI/CZIF-8. The pore diameter distributes from 2–60 nm, with a peak at 5.2 nm, which confirms the mesoporous structure of nZVI/CZIF-8[43, 44].

MB removal performances of CZIF-8 and nZVI/CZIF-8

MB solution (100 mL) with an initial concentration of 20 mg/L and adsorbent dosage of 0.02 g were used

to determine the MB removal performance of CZIF-8 with different particle sizes. As can be seen from Fig. 6a, the MB removal percentages with various particle sizes reach above 90% within 60 min, and then tend to be steady. The larger the particle size of CZIF-8 is, the shorter time to reach the maximal removal efficiency, which may be because the particles with smaller particle sizes have larger specific surface area and longer time to reach the maximal removal efficiency. Fig. 6b shows the MB removal percentages with different CZIF-8 doge. MB removal percentages increased gradually with the increase of adsorption time and CZIF-8 dosage and tended to be stable when the adsorption time exceeded 60 min.

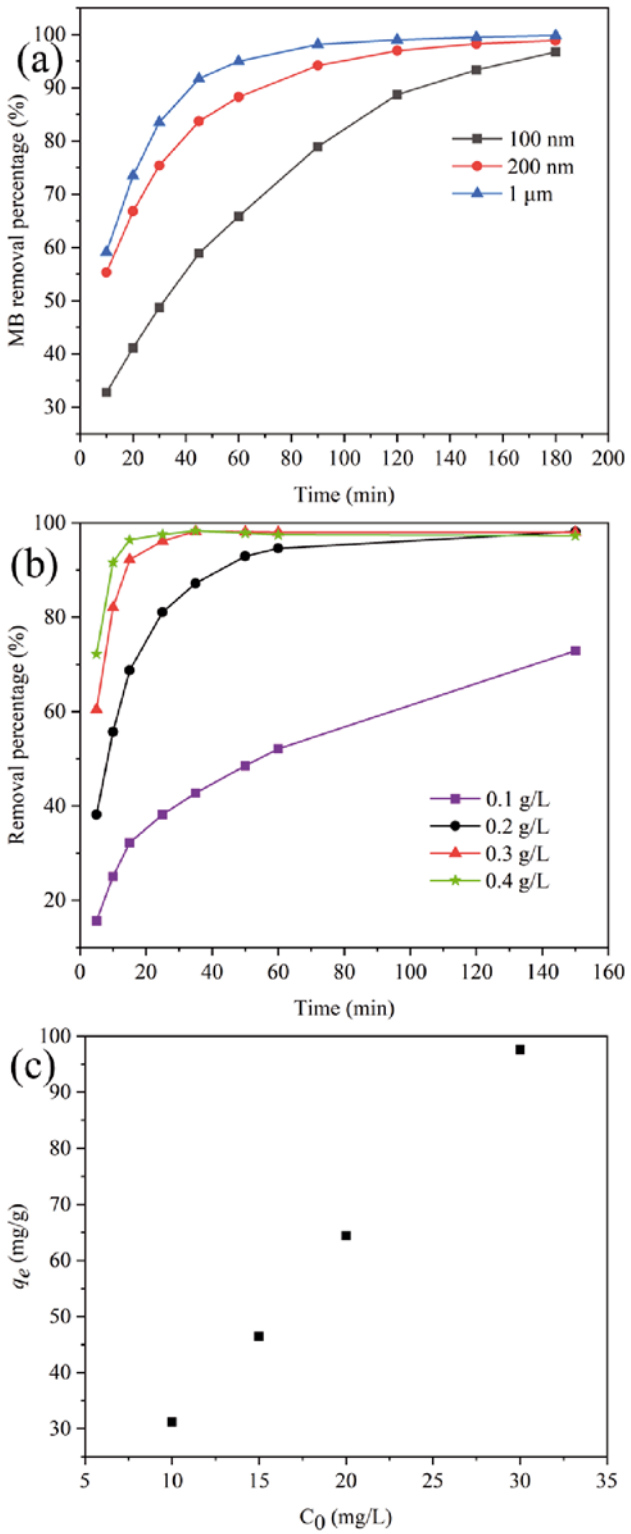

Figure 6. MB removal performances with different CZIF-8 size (a), dosage (b) and MB concentration (c)

The reason is that when the dosage of CZIF-8 is higher, it can provide more adsorption sites for MB removal. When the adsorption time is 25 min, the MB removal percentage by adding 0.4 g/L adsorbent is 97.58%, which is only 1.37% higher than that of 0.3 g/L adsorbent. The unit adsorption capacity is 48.79 mg/g, lower than 64.14 mg/g when adding 0.3 g/L adsorbent, this may be caused by an excessive adsorbent at 0.4 g/L. When the initial MB concentration increases from 10 mg/L to 30 mg/L, the equilibrium adsorption capacity increases from 37.19 mg/g to 97.63 mg/g (Fig. 6c).

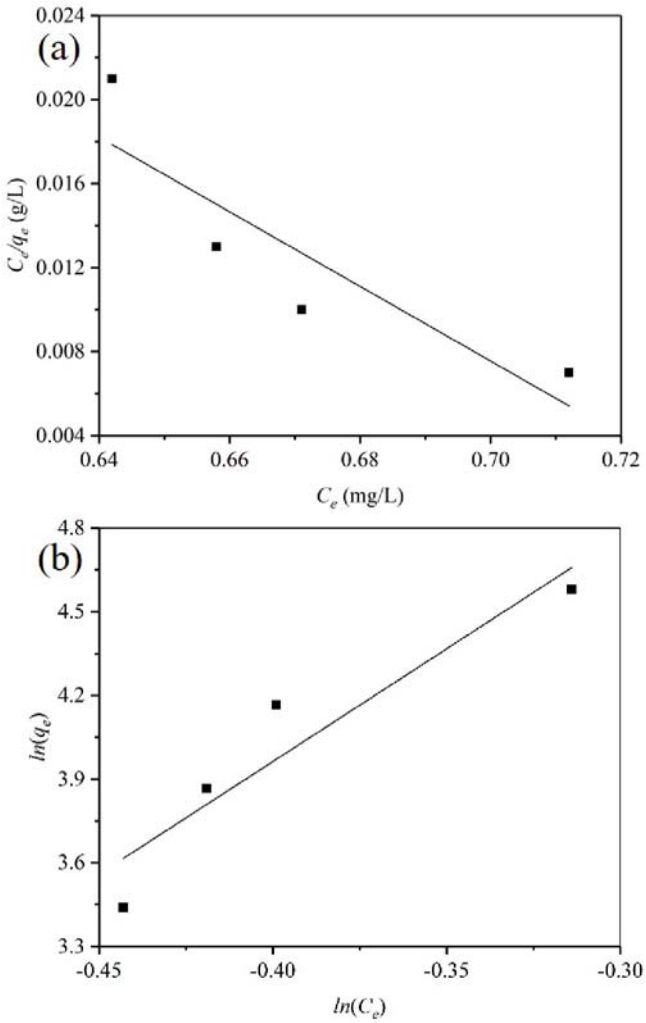

Figure 7. Fitting results of Langmuir (a) and Freundlich (b) adsorption models

Langmuir and Freundlich adsorption models were employed to analyze the adsorption mechanism, and the results were shown in Fig. 7. The Freundlich equation fits the MB adsorption data better than the Langmuir equation, and its correlation coefficient R^2 is 0.8878, which is higher than Langmuir equation's correlation coefficient (0.7816). In addition, the equilibrium constant K_L in the model is greater than 1, indicating that the adsorption reaction should not be carried out. The adsorption constant K_F in the Freundlich model is 1334.88 L/mol, implying that the material has a large adsorption capacity for MB. Therefore, the adsorption process of MB on CZIF-8 material is more consistent with the Freundlich model.

Figure 8a presents the comparison of MB removal performances between CZIF-8 and nZVI/CZIF-8. The MB removal percentage of CZIF-8 reached 74.5% at

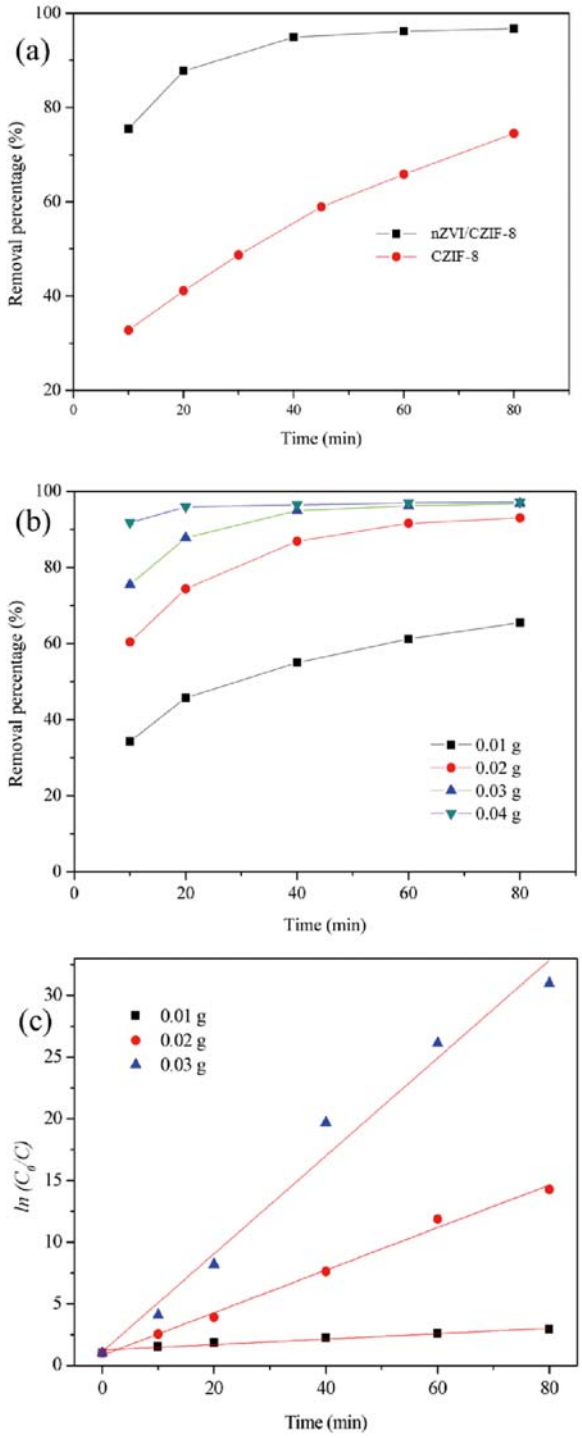

Figure 8. MB Removal performance of ZIF-8 and nZVI/CZIF-8 (a), effects of nZVI/CZIF-8 dosage on MB removal (b), and fitting results of pseudo-first-rate model (c)

80 min, while that of nZVI/CZIF-8 reached 96.2%. This may be due to the MB removal performance of nZVI[24]. Fig. 8b shows the effect of nZVI/CZIF-8 dosages on MB removal. The overall trend of MB removal by nZVI/CZIF-8 composites with different dosages can be found. At the initial stage, the removal percentage increased significantly and finally reached equilibrium in 80 min. The MB removal percentage increased with the increase of nZVI/CZIF-8 dosage. When the dosage was 0.01 g, the removal rate of MB was 65.5% in 80 min. As the dosage of nZVI/CZIF-8 increased to 0.02 g, the removal rate of MB in the solution was 93% at 80 min. Moreover, the MB removal percentages of 96.8% and 97.2% as the nZVI/CZIF-8 dosage reached 0.03 g and 0.04 g, respectively. MB removal by nZVI/CZIF-8 may contain both adsorption and oxidation by nZVI in water according to Eq. 7 and Eq. 8[47]Xiaohong</author><author>Sun, Yuankui</author><author>Qin, Hejie</author><author>Li, Jinxiang</author><author>Lo, Irene M. C.</author><author>He, Di</author><author>Dong, Haoran</author></authors></contributors><titles><title>The limitations of applying zero-valent iron technology in contaminants sequestration and the corresponding countermeasures: The development in zero-valent iron technology in the last two decades (1994–2014. The removal of MB by nZVI/CZIF-8 fits the pseudo-first-rate kinetic model well, and the results are summarized in Fig. 8c and Table 2, the MB removal rate reached 0.397 min^{-1} with the nZVI/CZIF-8 dosage of 0.03 g. Table 3 presents the comparison of MB removal performance of this study with previous studies. nZVI/CZIF-8 exhibits competitive removal performance of MB compared with previous studies.

$$Fe^0 + O_2 + 2H^+ \rightarrow Fe^{2+} + H_2O_2 \quad (7)$$

$$Fe^{2+} + H_2O_2 \rightarrow Fe^{3+} + \cdot OH + OH^- \quad (8)$$

Table 2. Fitting results of pseudo-first order reaction kinetics of different nZVI/CZIF-8 dosages

nZVI/CZIF-8 dosages (g)	k (min^{-1})	R^2
0.01	0.022	0.944
0.02	0.172	0.993
0.03	0.397	0.977

CONCLUSION

nZVI/CZIF-8 with high removal performance for MB was synthesized with $Fe(NO_3)_3 \cdot 9H_2O$ and ZIF-8. The adsorbents were prepared by a simple carbothermic reduction process, in which the formation of nZVI and the carbonization of ZIF occur simultaneously and nZVI is supported stable in the material. nZVI/CZIF-8 showed better MB removal performance than CZIF-8. The

Table 3. MB removal by various techniques from the literature

Materials	Removal capacity (mg/g)	Method	Reference
hickory chip biochar	10.1	Adsorption	9
$Na_2Ti_3O_7$	49.58	Adsorption	12
alginate/graphene oxide composite	12.64	Adsorption	15
clay	0.34	Adsorption	16
Native *C. equisetifolia* pine	41.35	Adsorption	17
ZIF-8/MCM-41	87.54	Adsorption	18
nZVI	96.5	Adsorption	24
Fe^0–Fe_3O_4–RGO	49	Oxidation	25
MPal/NZVI/CN	166.7	Photocatalytic reaction	26
Activated lignin-chitosan extruded blends	36.3	Adsorption	48
nZVI/CZIF-8	131	Adsorption and oxidation	This study

Freundlich equation fits the MB adsorption data better than the Langmuir equation. The adsorption constant KF in the Freundlich model is 1334.88 L/mol, indicating that the material has a large adsorption capacity for methylene blue. The MB removal percentages increase with increasing nZVI/CZIF-8 dosage, and the MB removal kinetic fits the pseudo-first rate kinetic model well. This study confirms the possibility of synthesizing active and stable nZVI/CZIF-8 in one step and its application to remove pollutants in water.

ACKNOWLEDGEMENTS

This work is supported by China Scholarship Council (202008310005), Shanghai Natural Science Foundation (21WZ2501500), National Natural Science Foundation of China (52070127), Program for Professor of Special Appointment (Eastern Scholar) at SIHL, Shanghai Engineering Research Center of Advanced Thermal Functional Materials and Gaoyuan Discipline of Shanghai-Materials Science and Engineering, Open Fund of Anhui International Joint Research Center for Nano Carbon-based Materials and Environmental Health (NCMEH2022Y02).

LITERATURE CITED

1. Rafatullah, M., Sulaiman, O., Hashim, R. & Ahmad, A. (2010). Adsorption of methylene blue on low-cost adsorbents: A review. *J. Hazard. Mater.,* 177, 70–80. DOI: 10.1016/j.jhazmat.2009.12.047.

2. Fadillah, G., Saleh, T.A., Wahyuningsih, S., Ninda Karlina Putri, E. & Febrianastuti, S. (2019). Electrochemical removal of methylene blue using alginate-modified graphene adsorbents. *Chem. Eng. J.,* 378, 122140. DOI: 10.1016/j.cej.2019.122140.

3. Zhang, P., O'Connor, D., Wang, Y., Jiang, L., Xia, T., Wang, L., Tsang, D.C.W., Ok, Y.S. & Hou, D. (2020). A green biochar/iron oxide composite for methylene blue removal. *J. Hazard. Mater.,* 384, 121286. DOI: 10.1016/j.jhazmat.2019.121286.

4. Salama, R.S., El-Sayed, E.-S.M., El-Bahy, S.M. & Awad, F.S. (2021). Silver nanoparticles supported on UIO-66 (Zr): As an efficient and recyclable heterogeneous catalyst and efficient adsorbent for removal of indigo carmine. *Colloid. Surface. A,* 626, 127089. DOI: 10.1016/j.colsurfa.2021.127089.

5. Alshorifi, F.T., Ali, S.L. & Salama, R.S. (2022). Promotional synergistic effect of Cs–Au NPs on the performance of Cs–Au/$MgFe_2O_4$ catalysts in catalysis 3,4-dihydropyrimidin-2(1h)-ones and degradation of RhB dye. *J. Inorg. Organomet. P,* 32, 3765–3776. DOI: 10.1007/s10904-022-02389-8.

6. Alshorifi, F.T., Alswat, A.A. & Salama, R.S. (2022). Gold-selenide quantum dots supported onto cesium ferrite nanocomposites for the efficient degradation of rhodamine B. *Heliyon,* 8, 6. DOI: 10.1016/j.heliyon.2022.e09652.

7. Ghosh, D. & Bhattacharyya, K.G. (2002). Adsorption of methylene blue on kaolinite. *Appl. Clay Sci.,* 20, 295–300. DOI: 10.1016/S0169-1317(01)00081-3.

8. El-Hakam, S.A., Alshorifi, F.T., Salama, R.S., Gamal, S., El-Yazeed, W.S.A., Ibrahim, A.A. & Ahmed, A.I. (2022). Application of nanostructured mesoporous silica/bismuth vanadate composite catalysts for the degradation of methylene blue and brilliant green. *J. Mater. Res. Technol.,* 18, 1963–1976. DOI: 10.1016/j.jmrt.2022.03.067.

9. Zhang, Y., Zheng, Y., Yang, Y., Huang, J., Zimmerman, A.R., Chen, H., Hu, X. & Gao, B. (2021). Mechanisms and adsorption capacities of hydrogen peroxide modified ball milled biochar for the removal of methylene blue from aqueous solutions. *Bioresour. Technol.,* 337, 125432. DOI: 10.1016/j.biortech.2021.125432.

10. Santoso, E., Ediati, R., Kusumawati, Y., Bahruji, H., Sulistiono, D.O. & Prasetyoko, D. (2020). Review on recent advances of carbon based adsorbent for methylene blue removal from waste water. *Mate. Today Chem.,* 16, 100233. DOI: 10.1016/j.mtchem.2019.100233.

11. Güleç, F., Williams, O., Kostas, E.T., Samson, A., Stevens, L.A. & Lester, E. (2022). A comprehensive comparative study on methylene blue removal from aqueous solution using biochars produced from rapeseed, whitewood, and seaweed via different thermal conversion technologies. *Fuel,* 330, 125428. DOI: 10.1016/j.fuel.2022.125428.

12. Reyes-Miranda, J., Garcia-Murillo, A., Garrido-Hernández, A.& Carrillo-Romo, F.d.J. (2021). Fast and mild alkaline solvothermal synthesis of nanostructured flower-like $Na_2Ti_3O_7$ and its methylene blue adsorption capacity. *Mater. Lett.,* 292, 129589. DOI: 10.1016/j.matlet.2021.129589.

13. Zhang, Z., Xu, L., Liu, Y., Feng, R., Zou, T., Zhang, Y., Kang, Y.& Zhou, P. (2021). Efficient removal of methylene blue using the mesoporous activated carbon obtained from mangosteen peel wastes: Kinetic, equilibrium, and thermodynamic studies. *Micropor. Mesopor. Mat.,* 315, 110904. DOI: 10.1016/j.micromeso.2021.110904.

14. Dai, K., Zhao, G., Kou, J., Wang, Z., Zhang, J., Wu, J., Yang, P., Li, M., Tang, C., Zhuang, W.& Ying, H. (2021). Magnetic mesoporous sodium citrate modified lignin for improved adsorption of calcium ions and methylene blue from aqueous solution. *J. Environ. Chem. Eng.,* 9, 105180. DOI: 10.1016/j.jece.2021.105180.

15. Ajeel, S.J., Beddai, A.A. & Almohaisen, A.M.N. (2021). Preparation of alginate/graphene oxide composite for methylene blue removal. *Mater. Today: Proc.*, DOI: 10.1016/j.matpr.2021.05.331.

16. Sharma, P., Olufemi, A.F. & Qanungo, K. (2021). Development of green geo-adsorbent pellets from low fire clay for possible use in methylene blue removal in aquaculture. *Mater. Today: Proc.*, DOI: 10.1016/j.matpr.2021.07.343.

17. Chandarana, H., Senthil Kumar, P., Seenuvasan, M. & Anil Kumar, M. (2021). Kinetics, equilibrium and thermodynamic investigations of methylene blue dye removal using casuarina equisetifolia pines. *Chemosphere,* 285, 131480. DOI: 10.1016/j.chemosphere.2021.131480.

18. Ibrahim, A.A., Salama, R.S., El-Hakam, S.A., Khder, A.S. & Ahmed, A.I. (2021). Synthesis of sulfated zirconium supported MCM-41 composite with high-rate adsorption of methylene blue and excellent heterogeneous catalyst. *Colloid. Surface. A,* 616, 126361. DOI: 10.1016/j.colsurfa.2021.126361.

19. Pasinszki, T., Krebsz, M., Chand, D., Kótai, L., Homonnay, Z., Sajó, I.E. & Váczi, T. (2020). Carbon microspheres decorated with iron sulfide nanoparticles for mercury(II) removal from water. *J. Mater. Sci.,* 55, 1425–1435. DOI: 10.1007/s10853-019-04032-3.

20. Wang, G., Gao, G., Yang, S., Wang, Z., Jin, P. & Wei, J. (2021). Magnetic mesoporous carbon nanospheres from renewable plant phenol for efficient hexavalent chromium removal. *Micropor. Mesopor. Mat.,* 310, 110623. DOI: 10.1016/j.micromeso.2020.110623.

21. Krebsz, M., Pasinszki, T., Tung, T.T., Nine, M.J. & Losic, D. (2021). Multiple applications of bio-graphene foam for efficient chromate ion removal and oil-water separation. *Chemosphere,* 263, 127790. DOI: 10.1016/j.chemosphere.2020.127790.

22. Pasinszki, T., Krebsz, M., Kótai, L., Sajó, I.E., Homonnay, Z., Kuzmann, E., Kiss, L.F., Váczi, T. & Kovács, I. (2015). Nanofurry magnetic carbon microspheres for separation processes and catalysis: Synthesis, phase composition, and properties. *J. Mater. Sci.,* 50, 7353–7363. DOI: 10.1007/s10853-015-9292-6.

23. Chen, S., Belver, C., Li, H., Ren, L.Y., Liu, Y.D., Bedia, J., Gao, G.L. & Guan, J. (2018). Effects of pH value and calcium hardness on the removal of 1,1,1-trichloroethane by immobilized nanoscale zero-valent iron on silica based

supports. *Chemosphere,* 211, 102–111. DOI: 10.1016/j.chemosphere.2018.07.127.

24. Sawafta, R. & Shahwan, T. (2019). A comparative study of the removal of methylene blue by iron nanoparticles from water and water-ethanol solutions. *J. Mol. Liq.,* 273, 274–281. DOI: 10.1016/j.molliq.2018.10.010.

25. Yang, B., Tian, Z., Zhang, L., Guo, Y.& Yan, S. (2015). Enhanced heterogeneous fenton degradation of methylene blue by nanoscale zero valent iron (nZVI) assembled on magnetic Fe_3O_4/reduced graphene oxide. *J. Water Proc. Eng.,* 5, 101–111. DOI: 10.1016/j.jwpe.2015.01.006.

26. Zhang, J., Zhang, T., Liang, X., Wang, Y., Shi, Y., Guan, W., Liu, D., Ma, X., Pang, J., Xie, X., Hong, K. & Wu, Z. (2020). Efficient photocatalysis of Cr(VI) and methylene blue by dispersive palygorskite-loaded zero-valent iron/carbon nitride. *Appl. Clay Sci.,* 198, 105817. DOI: 10.1016/j.clay.2020.105817.

27. Zhang, N., Eric, M., Zhang, C., Zhang, J., Feng, K., Li, Y. & Wang, S. (2021). ZVI impregnation altered arsenic sorption by ordered mesoporous carbon in presence of Cr(VI): A mechanistic investigation. *J. Hazard. Mater.,* 414, 125507. DOI: 10.1016/j.jhazmat.2021.125507.

28. Xu, J., Wang, X., Pan, F., Qin, Y., Xia, J., Li, J. & Wu, F. (2018). Synthesis of the mesoporous carbon-nano-zero-valent iron composite and activation of sulfite for removal of organic pollutants. *Chem. Eng. J.,* 353, 542–549. DOI: 10.1016/j.cej.2018.07.030.

29. Chen, S., Li, Z., Belver, C., Gao, G., Guan, J., Guo, Y., Li, H., Ma, J., Bedia, J. & Wójtowicz, P. (2020). Comparison of the behavior of ZVI/carbon composites from both commercial origin and from spent Li-ion batteries and mill scale for the removal of ibuprofen in water. *J. Environ. Manage.,* 264, 110480. DOI: 10.1016/j.jenvman.2020.110480.

30. Shi, J., Wang, J., Wang, W., Teng, W. & Zhang, W.-x. (2019). Stabilization of nanoscale zero-valent iron in water with mesoporous carbon (nZVI@MC). *J. Environ. Sci.,* 81, 28–33. DOI: 10.1016/j.jes.2019.02.010.

31. Baikousi, M., Georgiou, Y., Daikopoulos, C., Bourlinos, A.B., Filip, J., Zbořil, R., Deligiannakis, Y. & Karakassides, M.A. (2015). Synthesis and characterization of robust zero valent iron/mesoporous carbon composites and their applications in arsenic removal. *Carbon,* 93, 636–647. DOI: 10.1016/j.carbon.2015.05.081.

32. Gadipelli, S. & Guo, Z.X. (2015). Tuning of ZIF-derived carbon with high activity, nitrogen functionality, and yield – A case for superior CO_2 capture. *Chem. Sus. Chem.,* 8, 2123–2132. DOI: 10.1002/cssc.201403402.

33. Aijaz, A., Fujiwara, N. & Xu, Q. (2014). From metal–organic framework to nitrogen-decorated nanoporous carbons: High CO_2 uptake and efficient catalytic oxygen reduction. *J. Am. Chem. Soc.,* 136, 6790–6793. DOI: 10.1021/ja5003907.

34. Sann, E.E., Pan, Y., Gao, Z., Zhan, S. & Xia, F. (2018). Highly hydrophobic ZIF-8 particles and application for oil-water separation. *Sep. Purif. Technol.,* 206, 186–191. DOI: 10.1016/j.seppur.2018.04.027.

35. Pérez-Miana, M., Reséndiz-Ordóñez, J.U. & Coronas, J. (2021). Solventless synthesis of ZIF-l and ZIF-8 with hydraulic press and high temperature. *Micropor. Mesopor. Mater.,* 328, 111487. DOI: 10.1016/j.micromeso.2021.111487.

36. Qu, Y., Qin, L. & Liu, X. (2023). Carbonized ZIF-8/chitosan biomass imprinted hybrid carbon aerogel for phenol selective removal from wastewater. *Carbohyd. Polym.,* 300, 120268. DOI: 10.1016/j.carbpol.2022.120268.

37. Jiang, X.-F., Wang, X.-B., Dai, P., Li, X., Weng, Q., Wang, X., Tang, D.-M., Tang, J., Bando, Y. & Golberg, D. (2015). High-throughput fabrication of strutted graphene by ammonium-assisted chemical blowing for high-performance supercapacitors. *Nano Energy,* 16, 81–90. DOI: 10.1016/j.nanoen.2015.06.008.

38. Stobinski, L., Lesiak, B., Malolepszy, A., Mazurkiewicz, M., Mierzwa, B., Zemek, J., Jiricek, P. & Bieloshapka, I. (2014). Graphene oxide and reduced graphene oxide studied by the XRD, TEM and electron spectroscopy methods. *J. Electron Spectrosc.,* 195, 145–154. DOI: 10.1016/j.elspec.2014.07.003.

39. Chen, S., Bedia, J., Li, H., Ren, L.Y., Naluswata, F. & Belver, C. (2018). Nanoscale zero-valent iron@mesoporous hydrated silica core-shell particles with enhanced dispersibility, transportability and degradation of chlorinated aliphatic hydrocarbons. *Chem. Eng. J.,* 343, 619–628. DOI: 10.1016/j.cej.2018.03.011.

40. Zhang, X., Lin, D. & Chen, W. (2015). Nitrogen-doped porous carbon prepared from a liquid carbon precursor for CO_2 adsorption. *RSC Adv.,* 5, 45136–45143. DOI: 10.1039/c5ra08014b.

41. Chen, X., Lu, K., Lin, D., Li, Y., Yin, S., Zhang, Z., Tang, M. & Chen, G. (2021). Hierarchical porous tubular biochar based sensor for detection of trace lead (II). *Electroanalysis,* 33, 473–482. DOI: 10.1002/elan.202060148.

42. Lu, K.C., Wang, J.K., Lin, D.H., Chen, X., Yin, S.Y. & Chen, G.S. (2020). Construction of a novel electrochemical biosensor based on a mesoporous silica/oriented graphene oxide planar electrode for detecting hydrogen peroxide. *Anal. Methods,* 12, 2661–2667. DOI: 10.1039/d0ay00430h.

43. Yin, S., Wang, J., Li, Y., Wu, T., Song, L., Zhu, Y., Chen, Y., Cheng, K., Zhang, J., Ma, X., Lin,D. & Chen, G. (2021). Macroscopically oriented magnetic core-regularized nanomaterials for glucose biosensors assisted by self-sacrificial label. *Electroanalysis,* 33, 2216–2225. DOI: 10.1002/elan.202100231.

44. Lin, D., Zhang, X., Cui, X. & Chen, W. (2014). Highly porous carbons with superior performance for CO_2 capture through hydrogen-bonding interactions. *RSC Adv.,* 4, 27414–27421. DOI: 10.1039/c4ra04545a.

45. Luan, Tran, B., Chin, H.-Y., Chang, B.K. & Chiang, A.S.T. (2019). Dye adsorption in ZIF-8: The importance of external surface area. *Micropor. Mesopor. Mater.,* 277, 149–153. DOI: 10.1016/j.micromeso.2018.10.027.

46. Yao, J., He, M., Wang, K., Chen, R., Zhong, Z. & Wang, H. (2013). High-yield synthesis of zeolitic imidazolate frameworks from stoichiometric metal and ligand precursor aqueous solutions at room temperature. *Cryst. Eng. Comm.,* 15, 3601–3606. DOI: 10.1039/C3CE27093A.

47. Guan, X., Sun, Y., Qin, H., Li, J., Lo, I.M.C., He, D. & Dong, H. (2015). The limitations of applying zero-valent iron technology in contaminants sequestration and the corresponding countermeasures: The development in zero-valent iron technology in the last two decades (1994–2014). *Water Res.,* 75, 224–248. DOI: 10.1016/j.watres.2015.02.034.

48. Albadarin, A.B., Collins, M.N., Naushad, M., Shirazian, S., Walker, G. & Mangwandi, C. (2017). Activated lignin-chitosan extruded blends for efficient adsorption of methylene blue. *Chem. Eng. J.,* 307, 264–272. DOI: 10.1016/j.cej.2016.08.089.